# Highly efficient transfer hydrogenation catalysis with tailored pyridylidene amide pincer ruthenium complexes

Philipp Melle,[1] Jan Thiede,[1] Daniela A. Hey,[1,2] and Martin Albrecht*[,1]

*In memoriam Anneke Krüger*

[1] Department für Chemie und Biochemie, Universität Bern, Freiestrasse 3, CH–3012 Bern, Switzerland.

[2] Fakultät für Chemie, Technische Universität München, Lichtenbergstrasse 4, 85748 Garching, Germany

* email: martin.albrecht@dcb.unibe.ch

**Key words:** ruthenium; pyridylidene amide; ligand design; transfer hydrogenation; high turnover catalysis

**Abstract**

The rational optimization of homogeneous catalysts requires ligand platforms that are easily tailored to improve catalytic performance. Here, we demonstrate that pyridylidene amides (PYAs) provide such a platform to custom-shape transfer hydrogenation catalysts to exceptional activity. Specifically, a series of *meta*-PYA pincer ligands with differently substituted PYA units has been synthezised and coordinated to ruthenium(II) centres to form bench-stable *tris*-acetonitrile complexes [Ru(R-PYA-pincer)$(MeCN)_3$]$(PF_6)_2$ (R = OMe, Me, H, Cl, $CF_3$). Analytic studies including $^1$H NMR spectroscopy, cyclic voltammetry, and X-ray crystallography reveal a direct influence of the substituents on the electronic properties of the ruthenium center. The complexes are active in the catalytic transfer hydrogenation of ketones, with activities directly encoded by the PYA substitution pattern. Their perfomance improves further upon exchange of an ancillary MeCN ligand with $PPh_3$. While complexes [Ru(R-PYA-pincer)$(PPh_3)(MeCN)_2$]$(PF_6)_2$ were only isolated for R = H, Me, an *in situ* protocol was developed to generate these complexes *in situ* for R = OMe, Cl, $CF_3$ by using a 1:2 ratio of the complexes and $PPh_3$. This *in situ* protocol together with a short catalyst pre-activation provided highly active catalytic systems. The most active pre-catalyst featured the methoxy-substituted PYA ligand and reached turnover frenquencies of 210,000 $h^{-1}$ under an exceptionally low catalyst loading of 25 ppm for the benchmark substrate benzophenone, representing one of the most active transfer hydrogenation systems known to date.

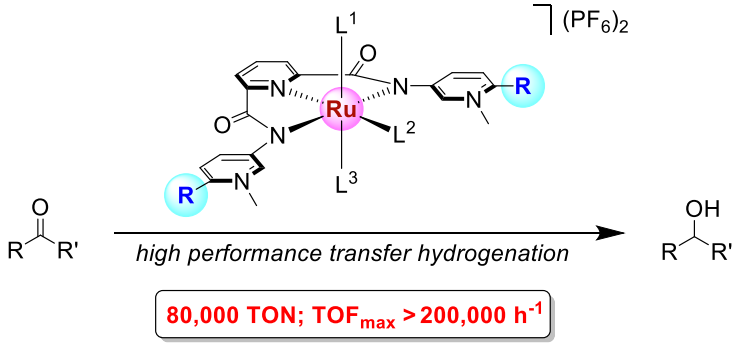

## Introduction

Advanced ligand design has become a key technology to improve homogeneous catalysts. Specifically, the development of cooperative ligands that undergo chemical transformation synergistically with the metal center has enabled numerous transformations with unrivalled efficiency.[1–8] In a complementary approach, considerable progress has been achieved with ligands that feature ambiguous donor properties. N-Heterocyclic carbenes (NHC) may be considered a prime example of this class of donor-ambiguous ligands, as NHCs feature a neutral L-type carbene resonance structure as well as an zwitterionic ylid resonance form, which imparts an anionic X-type metal coordination (**A**, Fig. 1).[9–12] Although rarely discussed in this context, this donor ambiguity of NHCs may be relevant for the high catalytic activity that these ligands often entail. A growing number of related ligand systems with a similarly ambiguous coordination motif has evolved from this scaffold, including for example mesoionic NHCs,[13,14] and N-heterocyclic olefins (**B**).[15–20] In more recent years, this concept has been expanded from C-donors to N-donor ligands as competitive alternatives to NHCs.[21] In particular Alcarazo-type ligand scaffolds combining a metal-bound imine as part of a guanidine derivative (**C**), or bound to a benzimidazolylidene or cyclopropenyl scaffold have shown promising donor properties.[22,23] A related ligand class are the so-called pyridylidene amides (PYAs, **D**)[24] and pyridylidene amines (PYEs),[25–27] which feature a neutral imine resonance structure with L-type metal coordination, as well as a zwitterionic pyridinium amide resonance form. These ligands were demonstrated to adapt their donor properties in response to the external environment, such as solvent polarity, and to the electronic configuration of the metal center, which ensues stabilization of different metal oxidation states.[28–30] As a consequence of these unique and flexible donor properties, PYA ligands have been successfully applied in a variety of catalytic transformations with appealing performances.[28–36]

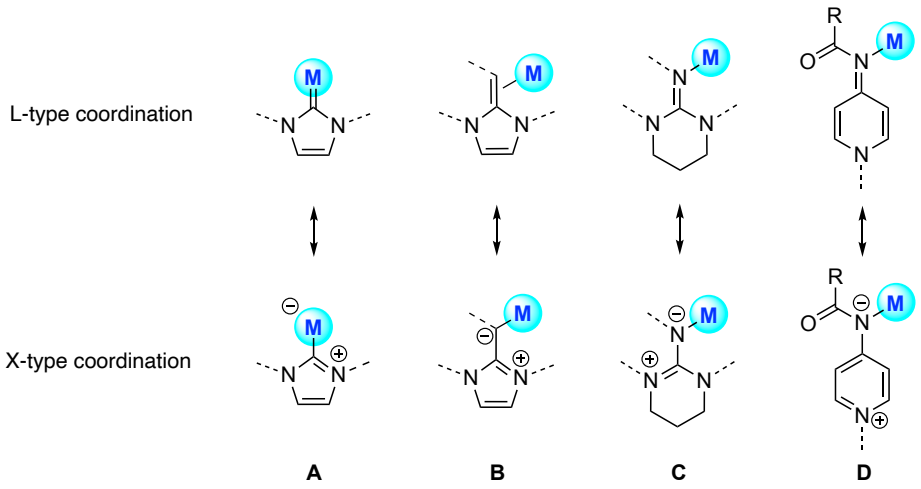


**Figure 1**. Selected ligands that feature ambiguous donor properties.

PYAs are a particularly attractive sub-class of donor-flexible ligands because of their easy accessibility and their synthetic versatility, which provides ample opportunities for ligand modifications. PYA variation has focused predominantly on modulation of the amide substituent R, including the incorporation of chelating groups,[24,28–30,35,37] as well as the positioning of the pyridinium site.[26,31,34,35] Remarkably, however, the synthetic versatility of pyridines has not been explored so far, even though such modifications are bound to have a direct impact on the donor properties of the PYA ligand. Here, we have introduced substituents on the PYA heterocycle in *meta*-PYA pincer-type ligands and demonstrate that their electronic influence directly affects the catalytic properties of the coordinated ruthenium center. We have exploited this methodology to develop highly active transfer hydrogenation catalysts, which reach turnover frequencies of more than 200,000 $h^{-1}$ and operate at unusually low catalyst loadings in the ppm range, thus providing a catalytic system that offers an attractive alternative to other high-performance catalysts.

## Results and discussion

**Synthesis of substituted PYA pincer ruthenium complexes.** The dicationic ligand salts **L1–5** were synthesized according to slightly modified literature procedures[38] starting from 2-substituted 5-aminopyridines and 2,6-pyridinedicarbonyl dichloride (Scheme 1). Amidation gave the substituted bis(amides) ***pre*-L1–5** in good 70–90% yields,[39] and subsequent methylation afforded the ligand precursors **L1–5**. Successful methlyation required an excess of MeOTf as a strong alkylating reagent rather than MeI, which was used for preparing the unsubstituted *meta*-PYA pincer ligand **L3**.[35] With MeI, an inseparable mixture of mono- and bis-alkylated products formed. Anion exchange from $OTf^-$ to $PF_6^-$ was accomplished with an excess of $NH_4PF_6$ in a $MeCN/H_2O$ solvent mixture, as indicated by HR ESI-MS analysis through detection of the monocationic ligand species, *e.g.* $[M–PF_6]^+$ at 554.1387 amu for **L1** (calcd. 554.1386).

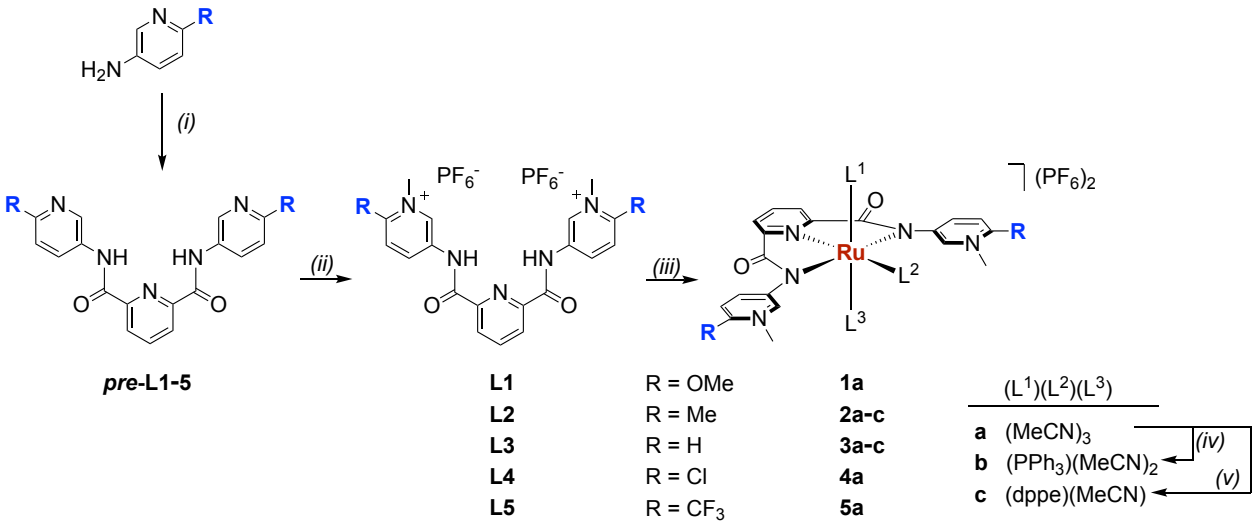


**Scheme 1.** General synthesis of the *para*-substituted *meta*-PYA pincer ligands, complexation to ruthenium, and ancillary ligand exchange. *Reagents and conditions*: *(i)* 2 eq. 2,6-pyridinedicarbonyl dichloride, toluene, reflux, 3h.

*(ii)* 3 eq. MeOTf, $CH_2Cl_2$, reflux, 16 h; then 5 eq. $NH_4PF_6$, $H_2O$/MeCN. *(iii)* 0.5 eq. $[RuCl_2(cym)]_2$, 3 eq. $Na_2CO_3$, MeCN, reflux, 16 h. *(iv)* 1.1 eq. $PPh_3$, EtOH, reflux 16 h. *(v)* 1.1 eq dppe, EtOH, reflux, 16 h.

Ruthenation of the ligand precursors **L1–5** was carried out with $[RuCl_2(cym)]_2$ under basic conditions (cym = *p*-cymene)[35] and gave the octahedral ruthenium(II) PYA pincer complexes **1a–5a** with ancillary MeCN ligands. The crude complexes were purified by conventional column chromatography to give analytically pure orange solids that were bench-stable for several weeks without requiring any protection from air or moisture. Ligand coordination to the $Ru^{II}$ center resulted in the loss of the low-field NH amide proton resonances and in a marked upfield shift of the aromatic $H^6_{PYA}$ proton resonances, *e.g.* from $\delta_H = 9.26$ in **L1** to 8.49 in complex **1a**. The three coordinated MeCN ligands gave two sets of singlets in 2:1 integral ratio, in agreement with two chemically equivalent axially coordinated MeCN entities and one equatorial MeCN coordinated in the PYA pincer plane.

Heating of the *tris*-acetonitrile complex **2a** comprised of a methyl-substituted PYA ligand in an ethanolic solution with a slight excess of $PPh_3$ or dppe (dppe = 1,2-diphenylphosphinoethane) afforded the monophosphine complex **2b** and the dppe analogue **2c**, respectively (Scheme 1). Remarkably, all attempts to isolate the phosphine variants of complexes **1**, **4** or **5** (R = OMe, Cl, $CF_3$) have been unsuccesful thus far. Neither modification of the synthetic procedure such as avoiding protic solvents, nor using lower temperatures or inert atmosphere, nor varying the phosphine equivalents gave the desired complexes. $^1$H NMR analysis of the crude products showed broad paramagnetic signals and attempts to isolate the formed products only gave insoluble black solids. We speculate that the Ru(II) complexes undergo a slow irreversible oxidation to form meta-stable Ru(III) species under the applied conditions.

**Spectroscopic, electrochemical, and structural analysis of the impact of the PYA substituents.** The electronic impact of the different PYA substituents of complexes **1a**–**5a** was indicated by a direct correlation of the $^1$H NMR chemical shifts of $H^3$ and $H^6$ of the PYA ligand with the Hammett parameter $\sigma_p$ of the corresponding substituent (Fig. S21, Table 1).[40] For example, the $H^3_{PYA}$ resonance shifts from $\delta_H = 7.37$ in complex **1** bearing a methoxy substituent ($\sigma_p = -0.27$) downfield to $\delta_H = 7.84$ in complex **3a** with an unsubstituted *meta*-PYA ligand ($\sigma_p = 0$) and to $\delta_H = 8.27$ in complex **5a** featuring an electron-withdrawing $CF_3$ substituent ($\sigma_p = +0.54$). A similar shift range of $\Delta\delta_H = 0.76$ was observed for the $H^6_{PYA}$ resonance, while the $H^4_{PYA}$ signal was unaffected, presumably due to H-bonding to the amide C=O fragment.

Whereas NMR spectroscopic data is limited to probe ligand-based electronic properties, cyclic voltammetry (CV) measurements provide a method to evaluate the electron density at the metal center. Complexes **1a**–**5a** show a reversible redox process around 0.5 V (*vs* SSCE) and a second, quasi-reversible process around 1.7 V (Fig. 2a, Fig. S22, S23), which have been attributed to $Ru^{II/III}$ and $Ru^{III/IV}$ transitions. The half-wave

potentials ($E_{1/2}$) for the $Ru^{II/III}$ oxidation indicate a direct influence of the substituent R on the oxidation potentials of complexes **1a–5a**. They gradually increase as the PYA substituent becomes less donating from 0.60 V for **1a** (R = OMe) to 0.66 V (complexes **2a** and **3a**, R = Me, H), 0.68 V (complex **4a**, R = Cl) and to 0.77 V (complex **5a**, R = $CF_3$). The qualitative correlation of the redox potential with the Hammett parameter $\sigma_p$ (Fig. 2b) indicates that the electron density at the metal center is rationally tailored by an appropriate choice of the substituent R in these PYA pincer ligands, revealing a substantial impact of synthetically simple ligand modifications. Moreover, it is remarkable that the potential window for the $Ru^{II/III}$ process ($\Delta E_{1/2}$ = 170 mV between R = OMe and R = $CF_3$) is considerably amplified for the $Ru^{III/IV}$ transition ($\Delta E_{1/2}$ = 310 mV).

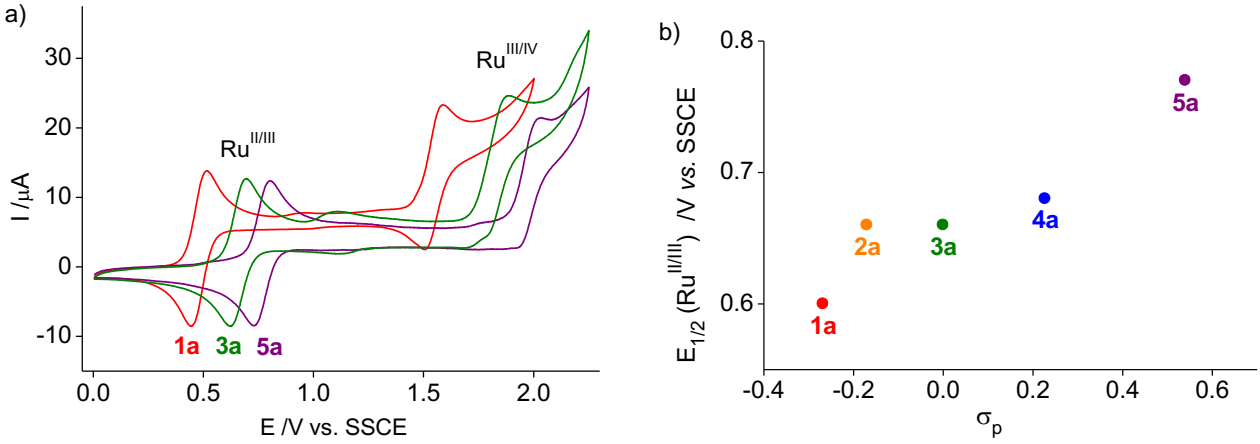


**Figure 2.** a) Cyclic voltammetry measurements of complexes **1a** (red), **3a** (green), and **5a** (purple) in MeCN (1 mM complex conc., potentials vs. SSCE using the $Fc^+/Fc$ couple as standard; $E_{1/2}$ = +0.4319 and n-$Bu_4NPF_6$ as electrolyte, 100 $mVs^{-1}$ scan rate). b) Redox potentials vs. $\sigma_p$ for complexes **1a**–**5a**.

Further support for the influence of the ligand system on the complex properties was gained by UV-vis spectroscopy (Fig. S24). The characteristic metal-to-ligand charge transfer (MLCT) bands in the visible region of the spectra (390–420 nm range) shift gradually to lower energy as the R-substituent becomes more electron withdrawing, in agreement with a lower energy of the ligand π* MOs and thus a smaller d−π* gap. Low-energy MLCT transitions indicate *π*-acidic properties of the PYA ligand and hence a pronounced imine rather than amide resonance form and L-type coordination (*cf* Fig. 1) when functionalized with electron-withdrawing Cl or $CF_3$ substituents.

**Table 1**. Selected $^{1}$H NMR, UV-vis spectroscopic and electrochemical data for complexes **1a–5a**

| entry | complex | R | $(L^1)(L^2)(L^3)$ | $\sigma_p$ | δ [ppm][a] | | $\lambda_{max}$ [nm][b] | $E_{1/2}$ [V][c] | |
|---|---|---|---|---|---|---|---|---|---|
| | | | | | $H^3$ | $H^6$ | | $Ru^{II/III}$ | $Ru^{III/IV}$ |
| 1 | **1a** | OMe | $(MeCN)_3$ | –0.27 | 7.37 | 8.49 | 393 | 0.60 | 1.67 |
| 2 | **2a** | Me | $(MeCN)_3$ | –0.17 | 7.70 | 8.83 | 397 | 0.66 | 1.79 |
| 3 | **3a** | H | $(MeCN)_3$ | 0.00 | 7.84 | 8.91 | 402 | 0.66 | 1.81 |
| 4 | **4a** | Cl | $(MeCN)_3$ | 0.23 | 7.92 | 9.03 | 405 | 0.68 | 1.83 |
| 5 | **5a** | $CF_3$ | $(MeCN)_3$ | 0.54 | 8.27 | 9.25 | 416 | 0.77 | 1.98 |

[a] in $CD_3CN$ at 298 K, 300 MHz. [b] in MeCN solutions (50–100 μM Ru complex). [c] in MeCN containing 0.1 M $n$Bu$_4$N(PF$_6$) as supporting electrolyte at 100 mV s$^{-1}$ scan rate, potentials *vs*. SSCE using $Fc^+$/Fc as internal standard at $E_{1/2}$ = +0.4319 (ref [56]).

Single crystals of complexes **1a** and **5a** were analyzed by X-ray diffraction. The molecular structures confirmed the octahedral geometry of the Ru(II) center and the connectivity pattern deduced from solution analysis (Fig. 3). Both structures show meridional coordination of the PYA pincer ligand and bonding of three MeCN ligands, with very similar bond distances around the metal center, *i.e.* little structural variation is imparted by the electronic nature of the PYA substituents (Table 2). The PYA pincer bite angle is identical in both complexes (157.13(5)° and 157.41(7)° for **1a** and **5a**, respectively), and equal to the unsubstituted analogue **3a** (157.55(8)°). Notably, the OMe-substituted PYA heterocycles in complex **1a** are substantially twisted out of the plane of the central pyridine ring ($\theta$ = 45.5° and 47.9°) compared to complex **3a** with no substituent ($\theta$ = 34.9° and 41.8°)[35] and complex **5a** featuring $CF_3$ groups ($\theta$ = 29.4° and 42.6°). A larger dihedral angle indicates a low $\pi$ contribution to the $N_{PYA}$–$C_{pyridyl}$ bond (N1–C3) and hence only little conjugation between the PYA heterocycle and the metal-bound amide nitrogen. Consequently, the amide nitrogen is predominantly acting as an anionic X-type *N*-donor ligand, a feature that is most pronounced in complex **1a** with strongly donating OMe substituents and least with electron-withdrawing $CF_3$ groups on the PYA unit.

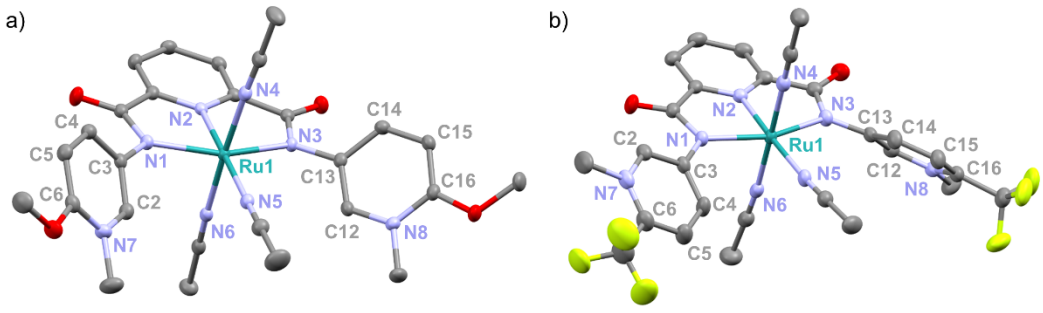

**Figure 3**. ORTEP representations of the complex cations **1a** (a) and **5a** (b); all ellipsoids at 50% probability level (hydrogen atoms, non-coordinating $PF_6^-$ anions and co-crystallized solvent molecules omitted for clarity).

**Table 2**. Selected bond lengths (Å) and angles (deg) for complexes **1a, 3a**, and **5a**

| | **1a** | **3a**[a] | **5a** |
|---|---|---|---|
| Ru1–N1 | 2.120(2) | 2.106(2) | 2.137(2) |
| Ru1–N2 | 1.966(1) | 1.959(2) | 1.964(2) |
| Ru1–N3 | 2.108(2) | 2.114(2) | 2.120(2) |
| Ru1–N4 | 2.009(2) | 2.024(2) | 2.022(2) |
| Ru1–N5 | 2.053(1) | 2.056(2) | 2.051(2) |
| Ru1–N6 | 2.015(2) | 2.010(2) | 2.022(2) |
| N1–Ru1–N3 | 157.13(5) | 157.55(8) | 157.41(7) |
| $\theta$ PYA–pyr [b] | 45.5; 47.9 | 34.9; 41.8 | 29.4; 42.6 |

[a] from ref [35]. [b] dihedral angle $\theta$ between the PYA heterocycle and the N–C=O amide plane.

**Transfer hydrogenation catalysis with isolated complexes.** All isolated complexes **1a**–**5a** were evaluated as catalyst precursors in transfer hydrogenation of benzophenone as model substrate. Under standard conditions (substrate/base/catalyst in 100:10:1 ratio in refluxing *i*PrOH),[41] all reactions went to completion within 1 h or less. The time-conversion profiles revealed turnover frequencies at 50% conversion, $TOF_{50}$, around 500 $h^{-1}$ for all complexes, though the unsubstituted complex **3a** featured a short induction period (Fig. 4, Table 3).

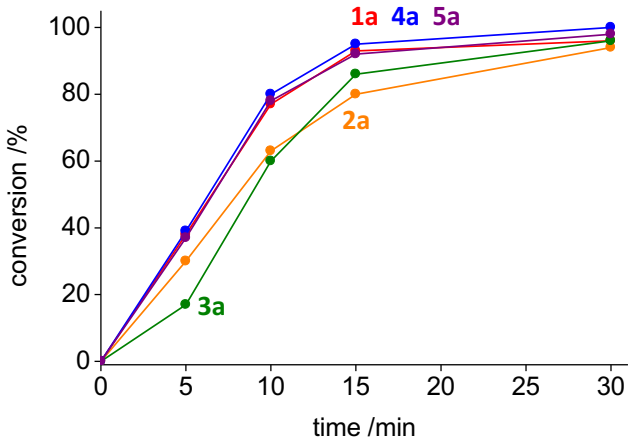


**Figure 4**. Time-conversion profiles for the transfer hydrogenation of benzophenone with complexes **1a** (red), **2a** (yellow), **3a** (green), **4a** (blue) and **5a** (purple). Reaction conditions: benzophenone (0.5 mmol), KOH (0.05 mmol, 10 mol%), cat. (0.005 mmol, 1 mol%), *i*PrOH (10 ml), $N_2$ atmosphere, reflux temperature.

Exchange of ancillary MeCN ligands by phosphines further enhanced the catalytic activity and allowed for reducing the catalyst loading to 0.1 mol% (entries 6–9). While the MeCN complex **2a** gave only slow conversion at this S/B/C ratio of 1000:10:1 (33% after 0.5 h; Fig. 5), introduction of dppe raised the activity markedly and complex **2c** reached 62% conversion within this time frame, corresponding to a 2-3 times better performance. Complex **2b** containing an ancillary $PPh_3$ ligand was even more active and reached full conversion within 30 min ($TOF_{50}$ around 7,000 $h^{-1}$). This activity is more than one order of magnitude higher than the MeCN analogue **2a**. This result underpins the benefits from combining the donor flexible PYA pincer scaffold with the strong *trans* effect of phosphine ligands[35,42] for efficient transfer hydrogenation catalysis.

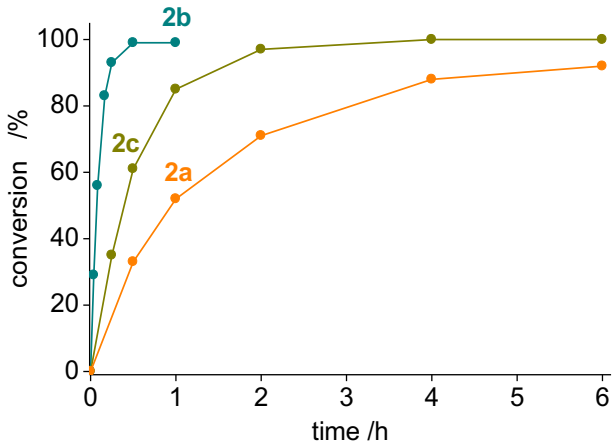


**Figure 5**. Time-conversion profiles for the transfer hydrogenation of benzophenone with complexes **2a** (orange), **2b** (cyan) and **2c** (light green) at 0.1 mol% catalyst loading. Reaction conditions: benzophenone (5.0 mmol), KOH (0.05 mmol, 10 mol%), cat. (0.005 mmol, 1 mol%), *i*PrOH (10 ml), $N_2$ atmosphere, reflux temperature.

**Table 3**. Catalytic activity of isolated PYA pincer ruthenium complexes in transfer hydrogenation of benzophenone.[a]

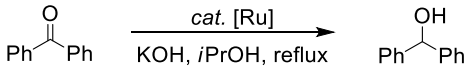


| entry | [Ru] | R | $(L^1)(L^2)L^3)$ | loading [mol%] | conversion [%][b] | | | | $TOF_{50}$ $[h^{-1}]$[c] |
|---|---|---|---|---|---|---|---|---|---|
| | | | | | 5 | 15 | 30 | 60 min | |
| 1 | **1a** | OMe | $(MeCN)_3$ | 1 | 38 | 93 | 96 | >99 | 470 |
| 2 | **2a** | Me | $(MeCN)_3$ | 1 | 30 | 80 | 94 | >99 | 380 |
| 3 | **3a** | H | $(MeCN)_3$ | 1 | 17 | 86 | 96 | >99 | 340 |
| 4 | **4a** | Cl | $(MeCN)_3$ | 1 | 39 | 95 | >99 | >99 | 480 |

| | | | | | | | | | |
|---|---|---|---|---|---|---|---|---|---|
| 5 | **5a** | $CF_3$ | $(MeCN)_3$ | 1 | 37 | 92 | 98 | >99 | 470 |
| 6 | **2a** | Me | $(MeCN)_3$ | 0.1 | n.d. | n.d. | 33 | 92 | 500 |
| 7 | **2b** | Me | $(PPh_3)(MeCN)_2$ | 0.1 | 56 | 93 | >99 | >99 | 6,900 |
| 8 | **2c** | Me | (dppe)(MeCN) | 0.1 | n.d. | 35 | 61 | >99 | 1,300 |
| 9 | **3b** | H | $(PPh_3)(MeCN)_2$ | 0.1 | 37 | 77 | 95 | >99 | 4,000 |

[a] General reaction conditions: benzophenone (0.5 or 5.0 mmol), KOH (0.05 mmol), [Ru] cat. (0.005 mmol), *i*PrOH (10 mL), $N_2$ atmosphere, reflux temperature. [b] Determined by $^1$H NMR spectroscopy using hexamethylbenzene as internal standard and averaged over two runs (less than 10% deviation), conversions correspond to yields; n.d. = not determined. [c] see SI for TOF calculations.

**Transfer hydrogenation catalysis with *in situ* formation of $PPh_3$ complexes.** Since all attempts to isolate the phosphine complexes $[Ru(R\text{-}PYA\text{-}pincer)(PPh_3)(MeCN)_2]^{2+}$ failed when the PYA unit was substituted with a OMe, Cl, or $CF_3$ group, an *in situ* methodology was developed to access complexes **1b**, **4b**, and **5b** for catalytic application. Such *in situ* strategies are widely used in homogeneous catalysis, *e.g.* in high throughput ligand screening[43–45] or when generating highly unstable catalytic systems.[46,47] The *in situ* methodology was validated with the *tris*-MeCN complex **3a** and compared with the catalytic activity of the analogous isolated $PPh_3$ complex **3b** at a S/B/C ratio of 1000:10:1 (Fig. 6). Thus, a catalytic run with complex **3a** in the presence of 2 eq. $PPh_3$ afforded a catalytic profile that is comparable to that of isolated complex **3b** apart from a short induction period, indicated by a mere 9% conversion after 5 min compared to 37% with the preformed complex **3b**. After this induction period, both catalytic systems showed essentially identical performance. Enhancing the phosphine concentration to 10 eq. gave lower conversion rates than with 2 equivalents. Presumably, competitive metal bonding disfavors substrate coordination and leads to complexes with more than one phosphine ligand, which lowers the catalytic performance (*cf* dppe complex **3c** and proposed mechanism in Scheme S1). This model is supported by the considerably lower activity when complex **3b** was used in the presence of 10 eq. $PPh_3$. The induction time was effectively suppressed, however, when complex **3a** was pre-activated with 2 eq. $PPh_3$ at 70°C for 10 min. These conditions reproduced the catalytic performance of the isolated complex **3b** very well and were therefore applied for catalysis with complexes **1a–5a** to generate complexes **1b–5b** *in situ*.

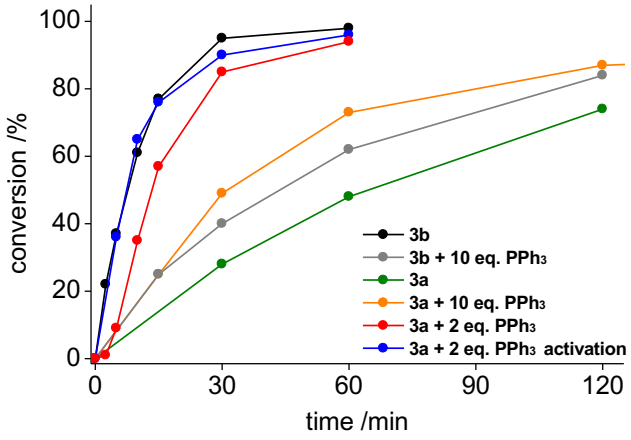


**Figure 6**. Time-conversion profiles for experiments carried out in order to find the best protocol for the *in situ* formation of catalyst **3b** starting from **3a**. General reaction conditions: benzophenone (5.0 mmol), KOH (0.05 mmol, 1 mol%), complex (0.005 mmol, 0.1 mol%), $PPh_3$ (varying amounts), *i*PrOH (10 ml), $N_2$ atmosphere, reflux temperature.

All pre-activated and *in situ* generated complexes **1b–5b** are considerably more active than the phosphine-free parent complexes **1a–5a**, and although the catalyst loading was reduced tenfold from 1 to 0.1 mol%, full conversion of benzophenone was achieved in much shorter reaction times than in the absence of $PPh_3$ at higher catalyst loading (Fig. 7, Table 4). For example, full conversion with complex **1a** requires more than 30 min at 1 mol% loading in the absence of $PPh_3$ (*cf* Table 3, entry 1), while the reaction is complete within 5 min at 0.1 mol% loading when 2 eq. $PPh_3$ were added (Table 4, entry 1). The activity of this system ($TOF_{max}$ about 20,000 $h^{-1}$) is almost two orders of magnitude higher than in the absence of phosphine ($TOF_{max}$ around 500 $h^{-1}$, *cf* Table 3). Pre-activation enhances the initial activity, though the maximum activity is unaltered (Table S1). Notably, the PYA substituents have a profound effect on the catalytic activity of the phosphine-activated complex. While a Me substituent did not change the activity of the ruthenium center significantly compared to the unsubstituted system, the $CF_3$ group in **5b** induced a twice higher activity, and complexes **1b** and **4b** with OMe and Cl substituents, respectively, displayed the highest activity of this series and reached $TOF_{max}$ around 20,000 $h^{-1}$. Obviously, the activity change is not governed solely by the Hammett $\sigma_p$ parameters of the different substituents and instead, other factors like inductive effects may play a significant role for catalytic turnover.

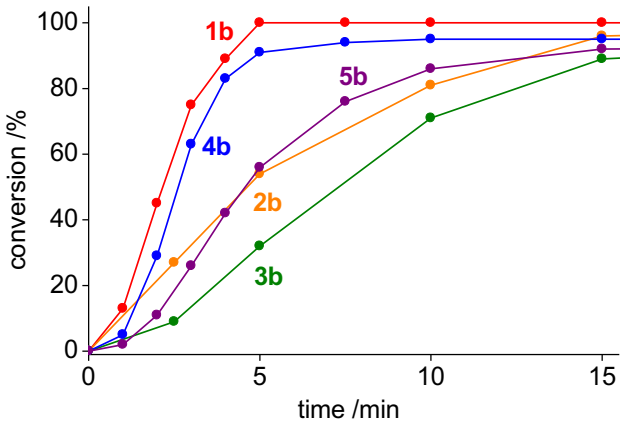


**Figure 7**. Time-conversion profiles for the transfer hydrogenation of benzophenone with *in situ* formation of $PPh_3$-complexes after pre-activation of the complex in the presence of 2 moleq. $PPh_3$ for 10 min at 70°C, **1b** (red), **2b** (yellow), **3b** (green), **4b** (blue) and **5b** (purple). Reaction conditions: benzophenone (5.0 mmol), KOH (0.05 mmol, 1 mol%), cat. (0.005 mmol, 0.1 mol%), $PPh_3$ (0.01 mmol, 0.2 mol%) *i*PrOH (10 ml), $N_2$ atm., reflux temperature.

**Table 4**. Catalytic activity in transfer hydrogenation of benzophenone for *in situ* formed complexes **1b–5b**.[a]

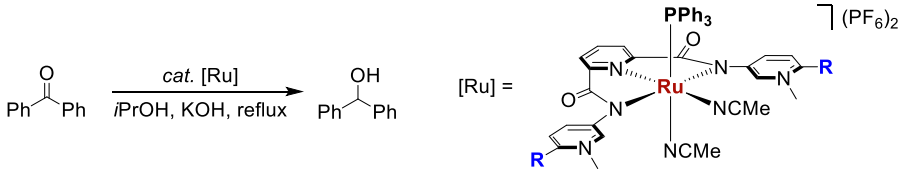


| entry | [Ru] | R | conversion [%][b] | | | | | $TOF_{max}$ [$h^{-1}$] |
|---|---|---|---|---|---|---|---|---|
| | | | 1’ | 2’ | 2.5’ | 5’ | 15’ | |
| 1 | **1b** | OMe | 13 | 45 | n.d. | >99 | >99 | 19,000 |
| 2 | **2b** | Me | n.d. | n.d. | 27 | 54 | 96 | 6,500 |
| 3 | **3b** | H | n.d. | n.d. | 9 | 32 | 89 | 5,500 |
| 4 | **4b** | Cl | 5 | 29 | n.d. | 91 | 95 | 14,000 |
| 5 | **5b** | $CF_3$ | n.d. | 11 | n.d. | 56 | 92 | 8,400 |

[a] General reaction conditions: benzophenone (5.0 mmol), complex **1a–5a** (0.005 mmol, 0.1 mol%), $PPh_3$ (0.01 mmol, 0.2 mol%) *i*PrOH (15 mL), $N_2$ atmosphere, at 70°C for 10 min, then KOH (0.05 mmol, 1 mol%), reflux temperature. [b] Determined by $^1H$ NMR spectroscopy using hexamethylbenzene as internal standard and averaged over two runs (less than 10% deviation), conversions correspond to yields.

**Catalytic transfer hydrogenation with complex 1b**. Since complex **1b** with OMe-substituted PYA units showed the highest catalytic activity within the series, it was used to optimize catalyst performance (Table 5). Benzophenone was still converted fully within 15 min when the catalyst loading was lowered by one order of magnitude to 0.01 mol% (entry 2). At 0.005 mol% catalyst loading full conversion required a twice longer reaction time (entry 3), and the time-conversion profile is almost identical to the reaction with

0.01 mol% of complex **1** (Fig. S26). Even at 0.0025 mol% catalyst loading (25 ppm) essentially full conversion was reached after 2 h (entry 4). Under these conditions, the $TOF_{max}$ was 210,000 $h^{-1}$, one of the highest activities noted for transfer hydrogenation and comparable to benchmark systems developed by Morris[48] (amine(imine)diphosphine iron complex, TOF = 140,000 $h^{-1}$ for benzophenone) or Baratta[49] (RuX(CO)(dppp)(NN)]Cl, TOF = 250,000 $h^{-1}$ for benzophenone). At a 10 ppm catalyst loading (0.001 mol%), conversion was substantially compromised and incomplete even after prolonging the reaction to 24 h, plateauing at 80% conversion (TON = 80,000, entry 5). The high TONs suggest a remarkable longevity of the catalytically active species, presumably imparted by the tridentate coordinating PYA pincer ligand. Similarly high TONs were reported with related tridentate ligands bound to ruthenium featuring either an S,N,Te-bonding motif (TON = 96,000)[50] or a CNC pincer-type bis(carbene) complex (TON = 126,000).[51] While attempts to also lower the base concentration from 1 to 0.1 mol% KOH resulted in negligible conversions even after longer reaction times (Fig. S26), the protocol is not restricted to benzophenone and also aliphatic and mixed aryl-alkyl ketones are successfully transfer hydrogenated with the the *in situ* formed complex **1b** (Fig. S27).

**Table 5**. Catalytic transfer hydrogenation activity of *in situ* formed complex **1b** towards benzophenone reduction [a]

| entry | **1b** [mol%] | time to equilibrium[b] | max. conversion [%][b] | $TOF_{max}$ [$h^{-1}$] | final TON [b] |
|---|---|---|---|---|---|
| 1 | 0.1 | 5 min | > 99 | 19,000 | > 990 |
| 2 | 0.01 | 15 min | > 99 | 90,000 | > 9,900 |
| 3 | 0.005 | 30 min | > 99 | 180,000 | > 19,800 |
| 4 | 0.0025 | 2 h | 98 | 210,000 | 39,200 |
| 5 | 0.001 | 24 h | 80 | 100,000 | 80,000 |

[a] General reaction conditions: benzophenone (10.0 mmol), cat. **1b** (x mol%), $PPh_3$ (2x mol%) *i*PrOH (15 mL), $N_2$ atmosphere, 70°C for 10 min, then KOH (0.1 mmol, 1 mol%), reflux temperature. [b] Determined by $^1H$ NMR spectroscopy using hexamethylbenzene as internal standard and averaged over two runs (less than 10% deviation), conversions correspond to yields.

**Conclusions**

Here, we demonstrate that modification of the PYA pincer ligand platform with substituents on the PYA fragment provides an efficient methodology for substantially improving ruthenium-catalyzed transfer hydrogenation. The introduction of substituents combined with an *in situ* protocol for the preparation of phosphine-containing complexes produces highly active systems that surpass the activity of the unsubstituted parent compounds by up to two orders of magnitude, reaching turnover frequencies around 200,000 $h^{-1}$, which is competitive to other state-of-the-art ruthenium-based catalysts. Moreover, the PYA pincer ruthenium complexes are active even at exceptionally low catalyst loading of 25 ppm. The 80,000

TON achieved with these complexes indicates a long-living catalytically active species. We speculate that the donor flexibility of the PYA ligand is particularly beneficial for accessing several transition states on the catalytic cycle and for stabilizing coordination of both neutral ketone and anioic hydride ligands required for classic monohydride transfer hydrogenation. The high catalyst performance is in line with the demanding requirements for precious metal catalysts and allows them to be used in small quantities only, underlining the potential of suitable ligand tailoring.

## Experimental

**General.** All reagents were commercially available and used as received. Compounds **L3**, and **3a–c** were synthesized according to previously described procedures.[35] Unless specified otherwise, NMR spectra were recorded at 298 K on Bruker spectrometers operating at 300 or 400 MHz ($^{1}$H NMR), and 100 MHz ($^{13}$C{$^{1}$H} NMR), respectively. Chemical shifts (δ in ppm, coupling constants *J* in Hz) were referenced to residual solvent signals ($^{1}$H, $^{13}$C). Assignments are based on homo- and heteronuclear shift correlation spectroscopy. Purity of bulk samples of the complexes has been established by NMR spectroscopy, and when possible by elemental analysis. Elemental analyses were performed at DCB Microanalytic Laboratory using a Thermo Scientific Flash 2000 CHNS-O elemental analyzer. High-resolution mass spectrometry was carried out with a Thermo Scientific LTQ Orbitrap XL (ESI-TOF) by the mass spectroscopy group of the Department of Chemistry and Biochemistry, University of Bern. UV/Vis measurements were performed on a UV-1800 spectrometer (Shimadzu) with 1 cm quartz cuvettes. Cyclic voltammograms were recorded using an Autolab PGSTAT101 from Metrohm in MeCN solutions using 10 mL solvent, 1 mM sample, and 100 mM tetrabutylammonium hexafluorophosphate ($n$Bu$_4$N)PF$_6$ as supporting electrolyte. Solutions were degassed with Ar gas for 10 min prior to each run. The scan rate was 100 mV s$^{-1}$. Redox potentials were measured using a Pt-button working electrode, an Ag/AgCl reference electrode (SSCE) and a Pt-wire auxiliary electrode and are tabulated versus a ferrocene internal standard. The Fc$^{+}$/Fc couple is 0.43 V vs. SSCE in 0.1 M ($n$Bu$_4$N)PF$_6$ MeCN solutions.[56]

**General procedure for the synthesis of ligands L1–5.** 2-6-Pyridinedicarbonyldichloride (1 eq.) and the corresponding 5-amino-2-substituted-pyridines (2.1–2.5 eq.) were heated to reflux in toluene under vigorous stirring for 3 h. After cooling to room temperature, the formed suspension was filtered and the residue washed with acetone, saturated $NaHCO_3$ solution, water, and again acetone. The resulting solid was dried at 80 °C and used for the methylation step without further purification. The solid was dissolved in dry $CH_2Cl_2$ under $N_2$ atmosphere and MeOTf (3 eq.) was added carefully. After heating the reaction mixture to reflux for 3–16 h, the reaction mixture was cooled to room temperature and residual MeOTf was quenched by adding MeOH (2–3 mL). The resulting precipitate was filtered, washed with small portions of $CH_2Cl_2$

and $Et_2O$, and air dried. This solid was then dissolved in a minimum amount of MeCN, and a solution of $NH_4PF_6$ (5 eq.) in $H_2O$ (twice the volume of MeCN) was added. The formed suspension was heated to reflux until a clear solution formed and then slowly cooled to room temperature, which resulted in the formation of crystals. After cooling to 6 °C for another 16 h, all crystals were filtered, washed with small portions of cold $H_2O$, and dried at 80 °C.

**Compound L1**. According to the general procedure starting from 2,6-pyridinedicarbonyldichloride (818 mg, 4 mmol) and 5-amino-2-methoxypyridine (1045 mg, 8.4 mmol) in toluene (60 mL) giving the bis-amide *N*$^2$,*N*$^6$-bis(6-methoxypyridin-3-yl)pyridine-2,6-dicarboxamide as a purple powder (1208 mg, 80%). Refluxing the bis-amide (1139 mg, 3.0 mmol) in dry $CH_2Cl_2$ (100 mL) with MeOTf (1.0 ml, 9 mmol) for 16 h gave **L1** as OTf salt (1621 mg, 75%). Reaction of this triflate salt (354 mg, 0.5 mmol) in MeCN (6 mL) with aqueous $NH_4PF_6$ (411 mg, 2.5 mmol) gave **L1** as light purple crystals (220 mg, 63%). $^1$H NMR (300 MHz, $CD_3CN$, 298 K): δ [ppm] = 10.36 (s, 2H, $NH_{amide}$), 9.25 (d, $^4J_{HH}$ = 2.6 Hz, 2H, $H_{PYA}$), 8.68 (dd, $^3J_{HH}$ = 9.5 Hz, $^4J_{HH}$ = 2.6 Hz, 2H, $H_{PYA}$), 8.50 (d, $^3J_{HH}$ = 7.8 Hz, 2H, $H_{pyr}$), 8.31 (t, $^3J_{HH}$ = 7.8 Hz, 1H, $H_{pyr}$), 7.58 (d, $^3J_{HH}$ = 9.5 Hz, 2H, $H_{PYA}$), 4.27 (s, 6H, $NCH_3$), 4.05 (s, 6H, $OCH_3$). HR ESI-MS ($CH_3CN$) *m/z* calculated for $[M–PF_6]^+$ = 554.1386; found: 554.1387. Elemental Analysis: calculated for $C_{21}H_{23}F_{12}N_5O_4P_2$: C: 36.07; H: 3.31; N: 10.01; found: C: 36.37; H: 2.55; N: 9.92.

**Compound L2**. According to the general procedure starting from 2,6-pyridinedicarbonyldichloride (611 mg, 3 mmol) and 5-amino-2-methylpyridine (811 mg, 7.5 mmol) in toluene (50 mL) giving the bis-amide *N*$^2$,*N*$^6$-bis(6-methylypyridin-3-yl)pyridine-2,6-dicarboxamide as a purple powder (896 mg, 86%). Refluxing the bis-amide (347 mg, 1.0 mmol) in dry $CH_2Cl_2$ (30 mL) with MeOTf (0.33 ml, 3 mmol) for 16 h gave **L2** as OTf salt (605 mg, 85%). Reaction of this triflate salt (271 mg, 0.4 mmol) in MeCN (6 mL), with aqueous $NH_4PF_6$ (329 mg, 2.0 mmol) gave **L2** as off white crystals (189 mg, 71%). $^1$H NMR (300 MHz, $CD_3CN$, 298 K): δ [ppm] = 10.52 (s, 2H, $NH_{amide}$), 9.57 (d, $^4J_{HH}$ = 2.3 Hz, 2H, $H_{PYA}$), 8.63 (dd, $^3J_{HH}$ = 8.8 Hz, $^4J_{HH}$ = 2.3 Hz, 2H, $H_{PYA}$), 8.53 (d, $^3J_{HH}$ = 7.7 Hz, 2H, $H_{pyr}$), 8.32 (t, $^3J_{HH}$ = 7.7 Hz, 1H, $H_{pyr}$), 7.91 (d, $^3J_{HH}$ = 8.8 Hz, 2H, $H_{PYA}$), 4.24 (s, 6H, $NCH_3$), 2.75 (s, 6H, $CH_3$). HR ESI-MS ($CH_3CN$) *m/z* calculated for $[M–PF_6]^+$ = 522.1488; found: 522.1484. Elemental Analysis: calculated for $C_{21}H_{23}F_{12}N_5O_2P_2$: C: 37.79; H: 3.47; N: 10.49; found: C: 37.53; H: 3.29; N: 10.10.

**Compound L4**. According to the general procedure starting from 2,6-pyridinedicarbonyldichloride (611 mg, 3 mmol) and 5-amino-2-chloropyridine (960 mg, 7.5 mmol) in toluene (50 mL) giving the bis-amide *N*$^2$,*N*$^6$-bis(6-chloroypyridin-3-yl)pyridine-2,6-dicarboxamide as a white powder (1013 mg, 87%). Refluxing the bis-amide (390 mg, 1.0 mmol) in dry $CH_2Cl_2$ (30 mL) with MeOTf (0.33 ml, 3 mmol) for 16 h gave **L4** as OTf salt (578 mg, 81%). Reaction of this triflate salt (359 mg, 0.5 mmol) in MeOH (36 mL) with solid $NH_4PF_6$ (818 mg, 5.0 mmol) **L4** as a white powder, which was washed with small portions of

cold MeOH (257 mg, 74%). $^1$H NMR (300 MHz, $CD_3CN$, 298 K): δ [ppm] = 10.65 (s, 2H, $NH_{amide}$), 9.75 (d, $^4J_{HH}$ = 2.5 Hz, 2H, $H_{PYA}$), 8.74 (dd, $^3J_{HH}$ = 9.1 Hz, $^4J_{HH}$ = 2.5 Hz, 2H, $H_{PYA}$), 8.54 (d, $^3J_{HH}$ = 7.8 Hz, 2H, $H_{pyr}$), 8.37–8.32 (m, 1H, $H_{pyr}$), 8.15 (d, $^3J_{HH}$ = 9.1 Hz, 2H, $H_{PYA}$), 4.39 (s, 6H, $NCH_3$). HR ESI-MS ($CH_3CN$) *m/z* calculated for $[M–PF_6]^+$ = 562.0396; found: 562.0406. Elemental Analysis: calculated for $C_{21}H_{17}Cl_2F_{12}N_5O_2P_2$: C: 32.22; H: 2.42; N: 9.89; found: C: 32.29; H: 3.03; N: 9.65.

**Compound L5**. According to the general procedure starting from 2,6-pyridinedicarbonyldichloride (310 mg, 1.5 mmol) and 5-amino-2-trifluoromethylpyridine (570 mg, 3.5 mmol) in toluene (25 mL) giving the bis-amide *N*$^2$,*N*$^6$-bis(6-trifluoromethylpyridin-3-yl)pyridine-2,6-dicarboxamide as a white powder (450 mg, 72%). Refluxing the bis-amide (300 mg, 0.66 mmol) in dry $CH_2Cl_2$ (40 mL) with MeOTf (0.22 ml, 2 mmol) for 16 h gave **L5** as OTf salt (479 mg, 93%). Reaction of this triflate salt (473 mg, 0.6 mmol) in MeCN (8 mL) with aqueous $NH_4PF_6$ (489 mg, 3.0 mmol) gave **L5** as white needle-like crystals (415 mg, 89%). $^1$H NMR (300 MHz, $CD_3CN$, 298 K): δ [ppm] = 10.86 (s, 2H, $NH_{amide}$), 9.86 (d, $^4J_{HH}$ = 2.3 Hz, 2H, $H_{PYA}$), 8.98 (dd, $^3J_{HH}$ = 8.9 Hz, $^4J_{HH}$ = 2.3 Hz, 2H, $H_{PYA}$), 8.59 (d, $^3J_{HH}$ = 7.8 Hz, 2H, $H_{pyr}$), 8.50 (d, $^3J_{HH}$ = 8.9 Hz, 2H, $H_{PYA}$), 8.38 (t, $^3J_{HH}$ = 7.8 Hz, 1H, $H_{pyr}$), 4.55 (s, 6H, $NCH_3$). HR ESI-MS ($CH_3CN$) *m/z* calculated for $[M–PF_6]^+$ = 630.0923; found: 630.0910. Elemental Analysis: calculated for $C_{21}H_{17}Cl_2F_{12}N_5O_2P_2$: C: 32.53; H: 2.21; N: 9.03; found: C: 32.59; H: 1.79; N: 9.01.

**General procedure for the synthesis of complexes 1a–5a.** The ligand **L1**–**L5** (1 eq.), $[RuCl_2(cym)]_2$ (0.5 eq.) and $Na_2CO_3$ (3 eq.) were dissolved in MeCN and heated to reflux for 16 h. The reaction mixture was cooled to –18 °C for 2 h for quantitative precipitation, then filtered over Celite and the filtrate was concentrated to a saturated solution under reduced pressure. The crude product was precipitated from $Et_2O$, filtered, washed with $Et_2O$, and purified by gradient column chromatography.

**Complex 1a**. According to the general procedure starting from **L1** (595 mg, 0.85 mmol), $[RuCl_2(cym)]_2$ (260 mg, 0.43 mmol) and $Na_2CO_3$ (274 mg, 2.55 mmol) in MeCN (180 mL). Purification by gradient column chromatography ($Al_2O_3$; $CH_2Cl_2$/MeCN 1:1 to pure MeCN) gave **1a** as dark orange powder (296 mg, 38%). $^1$H NMR (300 MHz, $CD_3CN$, 298 K): δ [ppm] = 8.49 (d, $^4J_{HH}$ = 2.5 Hz, 2H, $H_{PYA}$), 8.44 (dd, $^3J_{HH}$ = 9.3 Hz, $^4J_{HH}$ = 2.5 Hz, 2H, $H_{PYA}$), 8.04–8.00 (m, 3H, $H_{pyr}$), 7.37 (d, $^3J_{HH}$ = 9.3 Hz, 2H, $H_{PYA}$), 4.21 (s, 6H, $NCH_3$), 3.99 (s, 6H, $OCH_3$), 2.48 (s, 3H, $H_{MeCN(equ)}$), 2.13 (s, 6H, $H_{MeCN(axial)}$). $^{13}C\{^1H\}$ NMR (75 MHz, $CD_3CN$, 298 K): δ [ppm] = 170.73 (C=O), 158.09 ($C_{pyr}$), 156.43 ($C_{pyr}$), 146.66 ($CH_{pyr}$), 143.95 ($C_{pyr}$), 139.55 ($CH_{pyr}$), 136.82 ($CH_{pyr}$), 128.20 (N*C*Me), 125.81 ($CH_{pyr}$), 124.37 (N*C*Me), 110.12 ($CH_{pyr}$), 59.64 (O–$CH_3$), 42.48 (N–$CH_3$), 4.47 (NC*CH*$_3$), 4.11 (NC*CH*$_3$). HR ESI-MS ($CH_3CN$) *m/z* calculated for $[M–PF_6–MeCN]^+$ = 736.08043; found: 736.0809. Elemental Analysis: calculated for $C_{27}H_{30}F_{12}N_8O_4P_2Ru$: C: 35.19; H: 3.28; N: 12.16; found: C: 35.06; H: 3.51; N: 12.09.

**Complex 2a**. According to the general procedure starting from **L2** (154 mg, 0.24 mmol), $[RuCl_2(cym)]_2$ (71 mg, 0.12 mmol) and $Na_2CO_3$ (74 mg, 0.69 mmol) in MeCN (50 mL). No column chromatography was needed. Complex **2a** was isolated as dark orange powder (170 mg, 83%). $^1$H NMR (300 MHz, $CD_3CN$, 298 K): δ [ppm] = 8.83 (d, $^4J_{HH}$ = 2.2 Hz, 2H, $H_{PYA}$), 8.32 (dd, $^3J_{HH}$ = 8.7 Hz, $^4J_{HH}$ = 2.5 Hz, 2H, $H_{PYA}$), 8.08–8.03 (m, 3H, $H_{pyr}$), 7.69 (d, $^3J_{HH}$ = 8.7 Hz, 2H, $H_{PYA}$), 4.15 (s, 6H, $NCH_3$), 2.67 (s, 6H, $CH_3$), 2.47 (s, 3H, $H_{MeCN(equ)}$), 2.13 (s, 6H, $H_{MeCN(axial)}$). $^{13}C\{^1H\}$ NMR (75 MHz, $CD_3CN$, 298 K): δ [ppm] = 170.95 (C=O), 157.90 ($C_{pyr}$), 150.06 ($C_{pyr}$), 148.27 ($C_{pyr}$), 143.21 ($CH_{pyr}$), 142.72 ($CH_{pyr}$), 136.96 ($CH_{pyr}$), 129.04 ($CH_{pyr}$), 128.37 (N*C*Me), 126.20 ($CH_{pyr}$), 124.62 (N*C*Me), 46.69 (N–$CH_3$), 19.87 ($C_{PYA}$–*$CH_3$*), 4.51 (NC*$CH_3$*), 4.10 (NC*$CH_3$*). HR ESI-MS ($CH_3CN$) *m/z* calculated for $[M–PF_6–MeCN]^+$ = 704.0906; found: 704.0936. Elemental Analysis: calculated for $C_{27}H_{30}F_{12}N_8O_2P_2Ru \times 0.25\ CH_2Cl_2$: C: 35.93; H: 3.38; N: 12.30; found: C: 35.79; H: 3.90; N: 12.31.

**Complex 2b**. To a solution of **2a** (152 mg, 0.17 mmol) in EtOH (100 mL) was added $PPh_3$ (52 mg, 0.19 mmol) and the mixture was heated to reflux for 16 h. After cooling to RT, the solvent was removed under reduced pressure and the crude product was redissolved in a minimum amount of MeCN and precipitated from $Et_2O$, filtered, and washed with copious amounts of $Et_2O$. The residue was purified by gradient column chromatography ($Al_2O_3$; $CH_2Cl_2$/MeCN 1:1 to pure MeCN) to yield complex **2b** as an orange powder (102 mg, 54%). $^1$H NMR (300 MHz, 298 K): δ [ppm] = 8.24 (d, $^4J_{HH}$ = 2.2 Hz, 2H, $H_{PYA}$), 8.13 (dd, $^3J_{HH}$ = 8.5 Hz, $^4J_{HH}$ = 2.2 Hz, 2H, $H_{PYA}$), 7.75 (t, $^3J_{HH}$ = 7.7 Hz, 1H, $H_{pyr}$), 7.75 (d, $^3J_{HH}$ = 8.5 Hz, 2H, $H_{PYA}$), 7.58 (d, $^3J_{HH}$ = 7.7 Hz, 2H, $H_{pyr}$), 7.29–7.24 (m, 3H, $H_{PPh3}$), 7.03–6.99 (m, 6H, $H_{PPh3}$), 6.95–6.90 (m, 6H, $H_{PPh3}$), 4.00 (s, 6H, $NCH_3$), 2.72 (s, 6H, $CH_3$), 2.58 (s, 3H, $H_{MeCN(equ)}$), 2.12 (s, 3H, $H_{MeCN(axial)}$). $^{13}C\{^1H\}$ NMR (75 MHz, $CD_3CN$, 298 K): δ [ppm] = 170.14 (C=O), 156.30 ($C_{pyr}$), 150.07 ($C_{PYA}$), 148.37 ($C_{PYA}$), 144.15 ($CH_{PYA}$), 142.97 ($CH_{PYA}$), 136.76 ($CH_{pyr}$), 133.45 (d, $^2J_{CP}$ = 9.9 Hz, $CH_{PPh3}$), 132.61 (d, $^1J_{CP}$ = 44 Hz, $C_{PPh3}$), 130.66 (d, $^4J_{CP}$ = 2.2 Hz, $CH_{PPh3}$), 129.25 ($CH_{PYA}$), 128.98 (d, $^3J_{CP}$ = 9.3 Hz, $CH_{PPh3}$), 126.61 ($CH_{pyr}$), 46.51 (N–$CH_3$), 19.97 ($C_{PYA}$–*$CH_3$*), 5.24 (NC*$CH_3$*). $^{31}P\{^1H\}$ NMR (162 MHz, $CD_3CN$, 298 K): δ [ppm] = 51.86 (s, 1P, $PPh_3$), –144.59 (septett, $^1J_{PF}$ = 709 Hz, 2P, $PF_6$). HR ESI-MS ($CH_3CN$) *m/z* calculated for $[M–PF_6–2MeCN]^+$ = 884.1286; found: 884.1320. Elemental Analysis: calculated for $C_{43}H_{42}F_{12}N_7O_2P_3Ru \times CH_2Cl_2$: C: 44.20; H: 3.71; N: 8.20; found: C: 43.92; H: 3.42; N: 8.06.

**Complex 2c**. To a solution of **2a** (155 mg, 0.18 mmol) in EtOH (100 mL) was added dppe (80 mg, 0.20 mmol) in EtOH (100 ml) and the mixture was stirred at reflux for 16 h. After cooling to RT, the solvent was removed under reduced pressure and the crude product was redissolved in a minimum amount of MeCN and precipitated from $Et_2O$, filtered, and washed with copious amounts of $Et_2O$. The residue was purified by gradient column chromatography ($Al_2O_3$; $CH_2Cl_2$/MeCN 1:1 to pure MeCN) to yield complex **2c** as an orange powder (100 mg, 49%). $^1$H NMR (300 MHz, $CD_3CN$, 298 K): δ [ppm] = 8.41–8.37 (m, 1H, $H_{pyr}$), 8.23–8.21 (m, 2H, $H_{pyr}$), 7.35–7.31 (m, 2H, $H_{PPh}$), 7.29–7.17 (m, 14H, $H_{PPh}$ + $H_{PYA}$), 7.10–7.04 (m, 6H, $H_{PPh}$,

$H_{PYA}$), 6.84–6.78 (m, 4H, $H_{PPh}$, $H_{PYA}$), 3.65 (s, 6H, N–$CH_3$), 3.14–3.07 (m, 1H, $CH_2$), 3.05–3.02 (m, 1H, $CH_2$), 2.99–2.94 (m, 1H, $CH_2$), 2.92–2.86 (m, 1H, $CH_2$), 2.35 (s, 6H, $C_{PYA}$–$CH_3$). $^{13}C\{^1H\}$ NMR (75 MHz, $CD_3CN$, 298 K): δ [ppm] = 171.55 (C=O), 154.45 ($C_{pyr}$), 150.81 ($C_{PYA}$), 149.307 ($C_{PYA}$), 143.70 ($CH_{PYA}$), 143.08 ($CH_{PYA}$), 139.49 ($CH_{pyr}$), 136.42 (d, $^1J_{CP}$ = 36 Hz, $C_{PPh}$), 134.03 (d, $^1J_{CP}$ = 40 Hz, $C_{PPh}$), 131.21 (d, $J_{CP}$ = 9.0 Hz, $CH_{PPh}$), 131.05 (d, $J_{CP}$ = 8.1 Hz, $CH_{PPh}$), 130.83 (d, $J_{CP}$ = 2.2 Hz, $CH_{PPh}$), 129.89 (d, $J_{CP}$ = 8.8 Hz, $CH_{PPh}$), 129.68 (d, $J_{CP}$ = 2.3 Hz, $CH_{PPh}$), 129.29 (d, $J_{CP}$ = 8.7 Hz, $CH_{PPh}$), 129.14 ($CH_{PYA}$), 126.83 ($CH_{pyr}$), 46.17 (N–$CH_3$), 25.79–25.25 (m, $CH_{2dppe}$), 23.97–23.54 (m, $CH_{2dppe}$), 19.42 ($C_{PYA}$–*$CH_3$*). $^{31}P\{^1H\}$ NMR (162 MHz, $CD_3CN$, 298 K): δ [ppm] = 55.06 (d, $^1J_{PP}$ = 21 Hz, 1P, $P_{dppe}$), 54.47 (d, $^1J_{PP}$ = 21 Hz, 1P, $P_{dppe}$), –144.60 (hept, $^1J_{PF}$ = 707 Hz, 2P, $PF_6$). HR ESI-MS ($CH_3CN$) *m/z* calculated for $[M–PF_6–2MeCN]^+$ = 1020.1728; found: 1020.1758. Elemental Analysis: calculated for $C_{49}H_{48}F_{12}N_6O_2P_4Ru \times CH_2Cl_2$: C: 46.52; H: 3.90; N: 6.51; found: C: 47.10; H: 3.71; N: 6.41.

**Complex 4a**. According to the general procedure starting from **L4** (107 mg, 0.15 mmol), $[RuCl_2(cym)]_2$ (47 mg, 0.075 mmol) and $Na_2CO_3$ (48 mg, 0.45 mmol) in MeCN (40 mL). Purification by gradient column chromatography ($Al_2O_3$; $CH_2Cl_2$/MeCN 1:1 to pure MeCN) gave **4a** as red powder (90 mg, 65%). $^1H$ NMR (300 MHz, $CD_3CN$, 298 K): δ [ppm] = 9.02 (d, $^4J_{HH}$ = 2.5 Hz, 2H, $H_{PYA}$), 8.40 (dd, $^3J_{HH}$ = 9.0 Hz, $^4J_{HH}$ = 2.5 Hz, 2H, $H_{PYA}$), 8.11–8.06 (m, 3H, $H_{pyr}$), 7.92 (d, $^3J_{HH}$ = 9.0 Hz, 2H, $H_{PYA}$), 4.29 (s, 6H, $NCH_3$), 2.51 (s, 3H, $H_{MeCN(equ)}$), 2.13 (s, 6H, $H_{MeCN(axial)}$). $^{13}C\{^1H\}$ NMR (75 MHz, $CD_3CN$, 298 K): δ [ppm] = 171.21 (C=O), 157.48 ($C_{pyr}$), 151.07 ($C_{pyr}$), 145.06 ($CH_{pyr}$), 144.18 ($CH_{pyr}$), 138.30 ($C_{pyr}$), 137.16 ($CH_{pyr}$), 129.12 ($CH_{pyr}$), 128.93 (N*C*Me), 126.66 ($CH_{pyr}$), 124.94 (N*C*Me), 48.55 (N–$CH_3$), 4.62 (NC*$CH_3$*), 4.08 (NC*$CH_3$*). HR ESI-MS ($CH_3CN$) *m/z* calculated for $[M–PF_6–MeCN]^+$ = 743.9814; found: 743.9805. Elemental Analysis: calculated for $C_{25}H_{24}Cl_2F_{12}N_8O_2P_2Ru$: C: 32.27; H: 2.60; N: 12.04; found: C: 31.92; H: 2.61; N: 11.85.

**Complex 5a**. According to the general procedure starting from **L5** (293 mg, 0.38 mmol), $[RuCl_2(cym)]_2$ (116 mg, 0.19 mmol) and $Na_2CO_3$ (120 mg, 1.14 mmol) in MeCN (100 mL). Purification by gradient column chromatography ($Al_2O_3$; $CH_2Cl_2$/MeCN 1:1 to pure MeCN) gave **5a** as red powder (239 mg, 63%). $^1H$ NMR (300 MHz, $CD_3CN$, 298 K): δ [ppm] = 9.24 (d, $^4J_{HH}$ = 2.3 Hz, 2H, $H_{PYA}$), 8.51 (dd, $^3J_{HH}$ = 8.9 Hz, $^4J_{HH}$ = 2.3 Hz, 2H, $H_{PYA}$), 8.26 (d, $^3J_{HH}$ = 8.9 Hz, 2H, $H_{PYA}$), 8.20–8.09 (m, 3H, $H_{pyr}$), 4.42 (s, 6H, $NCH_3$), 2.55 (s, 3H, $H_{MeCN(equ)}$), 2.14 (s, 6H, $H_{MeCN(axial)}$). $^{13}C\{^1H\}$ NMR (75 MHz, $CD_3CN$, 298 K): δ [ppm] = 171.88 (C=O), 157.12 ($C_{pyr}$), 155.78 ($C_{pyr}$), 148.35 ($CH_{pyr}$), 141.44 ($CH_{pyr}$), 137.48 ($CH_{pyr}$), 131.73 ($CF_3$, q, $^1J_{CF}$ = 36.7 Hz), 129.60 (N*C*Me), 127.74 ($C_{pyr}$, q, $^2J_{CF}$ = 4.9 Hz), 127.41 ($CH_{pyr}$), 125.46 ($CH_{pyr}$), 122.02 (N*C*Me), 48.26 (N–$CH_3$), 4.76 (NC*$CH_3$*), 4.10 (NC*$CH_3$*). HR ESI-MS ($CH_3CN$) *m/z* calculated for $[M–PF_6–MeCN]^+$ = 812.0341; found: 812.0371. Elemental Analysis: calculated for $C_{27}H_{24}F_{18}N_8O_2P_2Ru$: C: 32.51; H: 2.43; N: 11.23; found: C: 32.44; H: 1.98; N: 10.71.

**General Procedure for Catalytic Transfer Hydrogenation.** In a 20 mL pressure tube, a mixture of the complex, 2 molequiv $PPh_3$ and hexamethylbenzene as internal standard were dissolved in *i*PrOH (5 mL). This solution was degassed with $N_2$ for 10 min. A degassed solution of the ketone substrate in *i*PrOH (1 M) was added via syringe and the solution was heated to 70 °C for 10 min. The catalytic reaction was started by injection of KOH (2 M solution in $H_2O$) and heated to reflux in an oil bath (110 °C). Aliquots (ca. 0.1 ml) were taken at set times, and quenched by dissolving into $CDCl_3$ for $^1H$ NMR analysis. Conversions were determined relative to hexamethylbenzene as internal standard and correspond to spectroscopic yields.

**Crystal structure determination.** Suitable single crystals of **1a** and **5a** were mounted in air at ambient conditions and measured on an Oxford Diffraction SuperNova area-detector diffractometer[57] using mirror optics monochromated Mo Kα radiation (λ = 0.71073 Å) and Al filtered.[58] The unit cell constants and an orientation matrix for data collection were obtained from a least-squares refinement of the setting angles of reflections. Data reduction was performed using the CrysAlisPro[57] program. The intensities were corrected for Lorentz and polarization effects, and a numerical absorption correction based on Gaussian integration over a multifaceted crystal model was applied. Data collection and refinement parameters are given in the SI. The structure was solved by direct methods using SHELXT[59], which revealed the positions of all non-hydrogen atoms of the title compounds. The non-hydrogen atoms were refined anisotropically. All H-atoms were placed in geometrically calculated positions and refined using a riding model where each H-atom was assigned a fixed isotropic displacement parameter with a value equal to 1.2Ueq of its parent atom (1.5$U_{eq}$ for methyl groups and water). Refinement of the structure was carried out on $F^2$ using full-matrix least-squares procedures, which minimized the function $\Sigma w(F_o^2 - F_c^2)^2$. The weighting scheme was based on counting statistics and included a factor to downweight the intense reflections. All calculations were performed using the *SHELXL-2014/7*[60] program in OLEX2.[61] The crystal of **1a** contains two co-crystallized acetonitrile solvent molecules and 0.173 co-crystallized water molecules per asymmetric unit. The crystal of **5a** contains one co-crystallized acetonitrile solvent molecule per asymmetric unit. Further crystallographic details are compiled in Tables S4 and S5. Crystallographic data for all structures have been deposited with the Cambridge Crystallographic Data Centre (CCDC) as supplementary publication numbers 1986022 (**1a**) and 1986021 (**5a**).

**Acknowledgements**

We thank the Swiss National Science Foundation (200020_182663) and the European Research Council (CoG 615653) for generous financial support and the Swiss European Mobility Programme for a visiting fellowship to D.A.H.

**Supporting Information:** NMR spectra of all compounds, cyclic voltammetry measurements of complexes **2a** and **4a**, UV-vis spectra of complexes **1a–5a**, catalytic transfer hydrogenation experiments, and crystallographic details.

**References**


[1] J. R. Khusnutdinova, D. Milstein, *Angew. Chem. Int. Ed.* **2015**, *54*, 12236–12273.

[2] C. Gunanathan, D. Milstein, *Chem. Rev.* **2014**, *114*, 12024–12087.

[3] C. Gunanathan, D. Milstein, *Acc. Chem. Res.* **2011**, *44*, 588–602.

[4] L. Alig, M. Fritz, S. Schneider, *Chem. Rev.* **2019**, *119*, 2681–2751.

[5] V. Lyaskovskyy, B. De Bruin, *ACS Catal.* **2012**, *2*, 270–279.

[6] L. A. Berben, B. De Bruin, A. F. Heyduk, *Chem. Commun.* **2015**, *51*, 1553–1554.

[7] J. I. Van Der Vlugt, *Eur. J. Inorg. Chem.* **2012**, 363–375.

[8] D. L. J. Broere, R. Plessius, J. I. Van Der Vlugt, *Chem. Soc. Rev.* **2015**, *44*, 6886–6915.

[9] D. Bourissou, O. Guerret, F. P. Gabbaï, G. Bertrand, *Chem. Rev.* **2000**, *100*, 39–91.

[10] M. N. Hopkinson, C. Richter, M. Schedler, F. Glorius *Nature* **2014**, *510*, 485–496.

[11] E. Peris, *Chem. Rev.* **2018**, *118*, 9988–10031.

[12] C. A. Smith, M. R. Narouz, P. A. Lummis, I. Singh, A. Nazemi, C. H. Li, C. M. Crudden, *Chem. Rev.* **2019**, *119*, 4986–5056.

[13] Á. Vivancos, C. Segarra, M. Albrecht, *Chem. Rev.* **2018**, *118*, 9493–9586.

[14] O. Schuster, L. Yang, H. G. Raubenheimer, M. Albrecht, *Chem. Rev.* **2009**, *109*, 3445–3478.

[15] N. Kuhn, H. Bohnen, J. Kreutzberg, D. Bläser, R. Boese, *J. Chem. Soc., Chem. Commun.* **1993**, 1136–1137.

[16] S. M. Ibrahim Al-Rafia, A. C. Malcolm, S. K. Liew, M. J. Ferguson, R. McDonald, E. Rivard, *Chem. Commun.* **2011**, *47*, 6987–6989.

[17] R. S. Ghadwal, S. O. Reichmann, F. Engelhardt, D. M. Andrada, G. Frenking, *Chem. Commun.* **2013**, *49*, 9440–9442.

[18] S. Naumann, *Chem. Commun.* **2019**, *55*, 11658–11670.

[19] M. M. D. Roy, E. Rivard, *Acc. Chem. Res.* **2017**, *50*, 2017–2025.

[20] E. Rivard, *Chem. Soc. Rev.* **2016**, *45*, 989–1003.

[21] L. Benhamou, E. Chardon, G. Lavigne, S. Bellemin-Laponnaz, V. César, *Chem. Rev.* **2011**, *111*, 2705–2733.

[22] H. Bruns, M. Patil, J. Carreras, A. Vμzquez, W. Thiel, R. Goddard, M. Alcarazo, *Angew. Chem. Int. Ed.* **2010**, *49*, 3680–3683.

[23] Á. Kozma, G. Gopakumar, C. Farès, W. Thiel, M. Alcarazo, *Chem. Eur. J.* **2013**, *19*, 3542–3546.

[24] P. D. W. Boyd, L. J. Wright, M. N. Zafar, *Inorg. Chem.* **2011**, *50*, 10522–10524.

[25] M. E. Doster, S. A. Johnson, *Angew. Chem. Int. Ed.* **2009**, *48*, 2185–2187.

[26] Q. Shi, R. J. Thatcher, J. Slattery, P. S. Sauari, A. C. Whitwood, P. C. McGowan, R. E. Douthwaite, *Chem. Eur. J.* **2009**, *15*, 11346–11360.

[27] J. Slattery, R. J. Thatcher, Q. Shi, R. E. Douthwaite, *Pure Appl. Chem.* **2010**, *82*, 1663–1671.

[28] K. F. Donnelly, C. Segarra, L.-X. Shao, R. Suen, H. Müller-Bunz, M. Albrecht, *Organometallics* **2015**, *34*, 4076–4084.

[29] M. Navarro, M. Li, H. Müller-Bunz, S. Bernhard, M. Albrecht, *Chem. Eur. J.* **2016**, *22*, 6740–6745.

[30] V. Leigh, D. J. Carleton, J. Olguin, H. Mueller-Bunz, L. J. Wright, M. Albrecht, *Inorg. Chem.* **2014**, *53*, 8054–8060.

[31] M. Navarro, M. Li, S. Bernhard, M. Albrecht, *Dalton Trans.* **2017**, *47*, 659–662.

[32] M. Navarro, C. A. Smith, M. Albrecht, *Inorg. Chem.* **2017**, *56*, 11688–11701.

[33] M. Navarro, C. A. Smith, M. Li, S. Bernhard, M. Albrecht, *Chem. Eur. J.* **2018**, *24*, 6386–6398.

[34] M. Navarro, V. Rosar, T. Montini, B. Milani, M. Albrecht, *Organometallics* **2018**, *37*, 3619–3630.

[35] P. Melle, Y. Manoharan, M. Albrecht, *Inorg. Chem.* **2018**, *57*, 11761–11774.

[36] P. Melle, M. Albrecht, *Chimia* **2019**, *73*, 299–303.

[37] C. M. A. Muller, M. V Babak, M. Kubanik, M. Hanif, S. M. F. Jamieson, C. G. Hartinger, L. J. Wright, *Inorg. Chim. Acta* **2016**, *450*, 124–130.

[38] A. Dorazco-González, H. Höpfl, F. Medrano, A. K. Yatsimirsky, *J. Org. Chem.* **2010**, *75*, 2259–2273.

[39] R. J. Thatcher, D. G. Johnson, J. M. Slattery, R. E. Douthwaite, *Chem. Eur. J.* **2012**, *18*, 4329–4336.

[40] C. Hansch, A. Leo, R. W. Taft, *Chem. Rev.* **1991**, *91*, 165–195.

[41] D. Wang, D. Astruc, *Chem. Rev.* **2015**, *115*, 6621–6686.

[42] B. J. Coe, S. J. Glenwright, *Coord. Chem. Rev.* **2000**, *203*, 5–80.

[43] M. Renom-Carrasco, L. Lefort, *Chem. Soc. Rev.* **2018**, *47*, 5038–5060.

[44] J. G. de Vries, A. H. M. de Vries, *Eur. J. Org. Chem.* **2003**, 799–811.

[45] M. R. Friedfeld, H. Zhong, R. T. Ruck, M. Shevlin, P. J. Chirik, *Science* **2018**, *360*, 888–893.

[46] C. Tai, J. Pitts, J. C. Linehan, A. D. Main, P. Munshi, P. G. Jessop, *Inorg. Chem.* **2002**, *41*, 1606–1614.

[47] J. Louie, R. H. Grubbs, *Angew. Chem. Int. Ed.* **2001**, *40*, 247–249.

[48] W. Zuo, A. J. Lough, Y. F. Li, R. H. Morris, *Science* **2013**, *342*, 1080–1084.

[49] S. Zhang, S. Baldino, W. Baratta, *Organometallics* **2013**, *32*, 5299–5304.

[50] P. Singh, A. K. Singh, *Organometallics* **2010**, *29*, 6433–6442.

[51] M. Poyatos, A. Mata, E. Falomir, R. H. Crabtree, E. Peris, *Organometallics* **2003**, *22*, 1110–1114.

[52] C. D. Nielsen, J. Bures, *Chem. Sci.* **2019**, *10*, 348–353.

[53] J. Bures, *Angew. Chem. Int. Ed.* **2016**, *55*, 2028–2031.

[54] J. Bures, *Angew. Chem. Int. Ed.* **2016**, *55*, 16084–16087.

[55] S. E. Clapham, A. Hadzovic, R. H. Morris, *Coord. Chem. Rev.* **2004**, *248*, 2201–2237.

[56] N. G. Connelly, W. E. Geiger, *Chem. Rev.* **1996**, *96*, 877–910.

[57] Oxford Diffraction Ltd., Ed., *CrysAlisPro*, Yarnton, Oxfordshire, U.K., **2010**.

[58] P. Macchi, H.-B. Bürgi, A. S. Chimpri, J. Hauser, Z. Gál, *J. Appl. Cryst.* **2011**, *44*, 763–771.

[59] G. M. Sheldrick, *Acta Crystallogr. C* **2015**, *71*, 3–8.

[60] G. M. Sheldrick, *Acta Crystallogr. A* **2015**, *71*, 3–8.

[61] O. V. Dolomanov, L. J. Bourhis, R. J. Gildea, J. A. K. Howard, H. Puschmann, *J. Appl. Cryst.* **2009**, *42*, 339–341.